Title
ON GEOMETRY OF TRACKS IN DIELECTRIC NUCLEAR TRACK DETECTORS

Authors
Henke, R.P.
Benton, E.V.

Publication Date
1971-06-01

Submitted to Nuclear
Instruments and Methods

UCRL-20852
Preprint

ON GEOMETRY OF TRACKS IN DIELECTRIC NUCLEAR TRACK DETECTORS

R. P. Henke and E. V. Benton
DONNER LABORATORY

June 1971

AEC Contract No. W-7405-eng-48

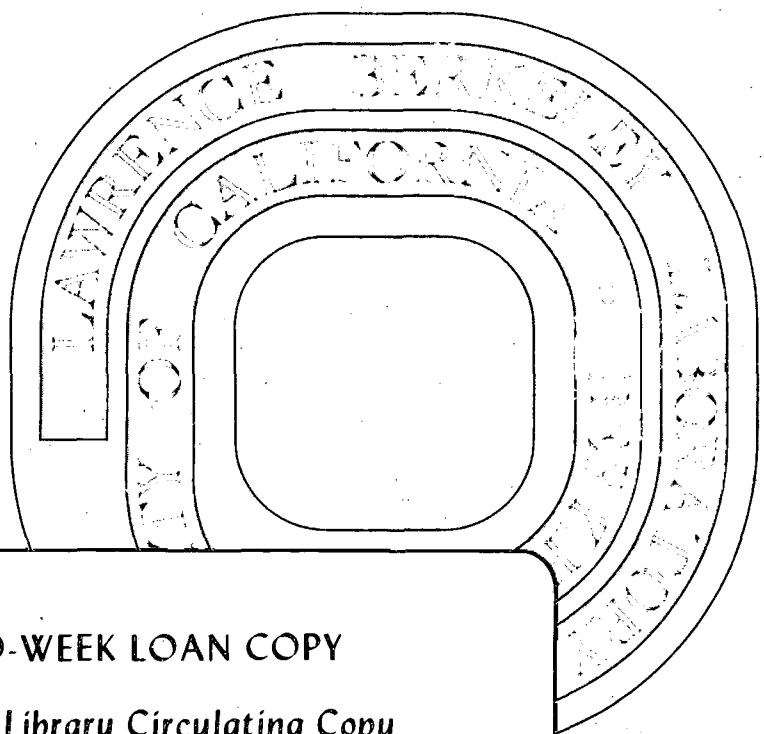

DISCLAIMER

ON GEOMETRY OF TRACKS IN DIELECTRIC NUCLEAR TRACK DETECTORS†

R. P. Henke* and E. V. Benton*

Donner Laboratory, Lawrence Radiation Laboratory
University of California, Berkeley, California 94720

Dielectric nuclear track detectors are now being utilized in a variety of research applications involving registration of heavily ionizing charged particles. Many situations call for the identification of particle charge Z, energy E, and possibly the mass M[1,2]. In these cases, a detailed knowledge of the etched track geometry is necessary to make possible computation of the relevant track parameters from the measured track features. Geometry of etched particle tracks can be quite complex. In this paper some of the most relevant aspects of track geometry are derived and discussed in considerable detail. Two basic assumptions are made: the detector is isotropic and homogeneous, and the particle ionization rate remains constant over the etched portion of the track. Track specification and measurement parameters are developed for a variety of different situations.

†Work supported by NASA, Ames Research Center and U. S. Atomic Energy Commission. A portion of this work was performed at the University of San Francisco and supported by NASA, G. C. Marshall Space Flight Center, under Contract NAS8-26758.

*Permanent address: Physics Department, University of San Francisco, San Francisco, California 94117.

1. Introduction

Chemical etching results in a preferential attack of the particle damage trail, producing regular geometric etch pits, which in most cases can be closely approximated by a cone with the damage trail as an axis. In some applications only the fluences (number/cm^2) of tracks are desired; in these it is necessary only to distinguish the tracks from the background etch pits. In many studies, however, parameters of the track-producing particle such as the particle trajectory length and the dip angle or the particle ionization rate must be known. In these cases, detailed knowledge of the track geometry is necessary in order to compute these parameters from track features that can be seen and measured with an optical microscope. In several recent publications certain "effects," which in reality are merely a consequence of normal track etching, have been attributed by investigators to other causes. It is clear that a detailed exposition of track geometry is needed to ensure the proper interpretation of track measurements.

2. Track etching process

On a submicroscopic scale, a particle damage trail and the subsequent formation of an etched track can be viewed in terms of the chemical attack of a very narrow linear region, as shown in fig. 1. On the right-hand side is shown the tip of a track resulting from a chemical attack of the damaged region. The degree of radiation damage is greatest in the immediate vicinity of the particle trajectory, and the etch rate (normal to the leading end of the etch pit) has its greatest value V_T, the track etch rate. The degree of damage and the etch rate both decrease as the distance from the trajectory

increases. At a certain distance (estimated to be somewhere between 25 and 50 Å) the damage falls off to some small value, and the etch rate normal to the interior of the track is the etch rate of the undamaged bulk material, V_G. Since the advancing tip of the etch pit maintains its shape while moving forward at a rate V_T in the undamaged region, the angle made by the walls of the etch pit with the particle trajectory must be such that the projection of V_T in the direction of the normal to these walls will be V_G. This is shown in the vector diagram of fig. 1. Consequently the track cone angle θ is given by

$$\sin\theta = (V_G/V_T). \qquad (1)$$

If one observes track formation on the scale of an optical microscope, the rounded tip shown in fig. 1 appears perfectly sharp. As the track tip proceeds past each point on the particle trajectory, the track walls expand, carrying with them a cone angle characteristic of V_T at this particular point [eq. (1)]. It has been found[3] that V_T can be expressed as a monotonically increasing function of the particle restricted energy loss rate REL_{ω_0}, the rate of energy loss to electrons with energies less than ω_0. The function REL is identical to the more commonly used function LET_{ω_0}. Thus as LET varies along the particle damage trail, V_T and θ also vary. This is illustrated in fig. 2.

In fig. 2a is shown formation of a track when etching proceeds from the direction of the particle stopping point. In fig. 2b the etching direction is the same as that of the particle travel. In both cases, the cone angle at point B is representative of the track etch rate at point A. As can be seen, the cone angle decreases toward the stopping end of the damage trail as LET and the track etch rate increase.

Although nearly all tracks have continuously varying cone angles (except for the case of very fast particles), it is mathematically expedient to approximate track shape by geometric cones. In most cases this is a good approximation, since the deviations from conical track structure are usually beyond the measurement capability when ordinary microscopes are used. When the deviation from conical track structure can be seen, the conical approximation can be taken to give average values of parameters such as θ. Consequently the remainder of this paper deals strictly with a conical track model. This is equivalent to assuming that LET is constant, that the detector is homogeneous and isotropic, and that the track and bulk etch rates are not affected by concentration gradients caused by the diffusion of either the etchant or the etch products.

3. Track evolution for the case of a stopping particle

The various stages of evolution of an etched track are shown in fig. 3, which is a side view of a track with dip angle $\delta = 45$ deg and cone angle $\theta = 15$ deg. The positions of the detector surface are labeled in a time sequence from 0 to 6. At time t_0, the surface of the detector is coincident with the top of the damage trail. For damage trails which entered or exited the detector surface, t_0 is the instant the detector first enters the etch bath. For damage trails completely contained within the detector, t_0 is the instant at which the etched detector surface just touches the end of the damage trail. For brevity, the surface at t_0 is called the pre-etch surface, even for "submerged" tracks.

After t_0, the detector surface is removed at a rate V_G, while the rate of attack along the damage trail is V_T. At time t_1, the

vertex of the track cone is pointed. The etch length of the track L, the distance to the cone vertex from the top of the damage trail, is given by

$$L = B \csc \theta, \tag{2}$$

where B is the bulk material removed since t_0. (fig. 4 shows the parameters of pointed tracks.) Equation (2) can be obtained by integrating eq. (1) with respect to time and realizing that

$$L = \int_{t_0}^{t} V_T \, dt \tag{3}$$

and

$$B = \int_{t_0}^{t} V_G \, dt . \tag{4}$$

The cone of cone angle θ intersecting the surface at a dip angle $\delta (> \theta)$ produces an elliptical surface opening--a conic section. Geometrical considerations give the semimajor axis of this surface ellipse $\underline{a}$ by

$$a = \frac{B \cos \theta}{\sin \delta + \sin \theta} . \tag{5}$$

and its semiminor axis $\underline{b}$ by

$$b = B \sqrt{\frac{\sin \delta - \sin \theta}{\sin \delta + \sin \theta}} . \tag{6}$$

At time t_2 the preferential etching is just complete. The track vertex is still pointed and the track is of the same geometry as at t_1. At $t > t_2$, further etching proceeds at a rate V_G (normal to all surfaces). This results in the rounding of the track vertex. The vertex becomes a sphere of radius r, given by

$$r = V_G (t - t_2), \tag{7}$$

and joins smoothly with the conical part of the track. At times greater than t_2, L continues to have the same value--which is called L_r, the length of the damage trail in this layer of the detector. This is shown in fig. 5, which shows the parameters of a rounded track.

At etch time t_3 [stage (3) of fig. 3], the track has developed a spherical tip of radius r. Equations (5) and (6) are still valid, but eq. (2) has become

$$B = L_r \sin \theta + r, \tag{8}$$

which reduces to eq. (2) if $r = 0$ and L_r is replaced by L. On the right-hand side of eq. (8), $L_r \sin \theta$ is the bulk etch that took place during the preferential etch, and r is the subsequent bulk etch. The depth from the surface to the bottom end of the damage trail is z, which is also the center of the vertex sphere (see fig. 5), and is given by

$$z = L_r \sin \delta - B. \tag{9}$$

[For pointed tracks, L_r in eq. (9) is replaced by L, and in this case z is the depth of the track vertex.] The total projected length of the track s, as shown in fig. 5, is now given by

$$s = L_r \cos \delta + r + B \tan \tfrac{1}{2} (\delta - \theta). \tag{10}$$

Equation (10) follows directly from the geometry as seen in fig. 5a. Equation (10) can also be used for pointed tracks by setting $r = 0$. It should be noted that the horizontal displacement of the "back" of the surface ellipse from the top of the damage trail, $B \tan \frac{1}{2} (\delta - \theta)$, is small compared with $\underline{a}$ [eq. (5)], except for large values of $(\delta - \theta)$.

At this point it is appropriate to discuss a special case--tracks that are not undercut. A track is undercut if the detector surface overhangs some portion of the track. For a track etched to stage (3), as shown in fig. 3, undercutting occurs if $\delta < (\pi/2 - \theta)$, s is no longer defined, and z and r cannot be observed from above as they can with $\delta < (\pi/2 - \theta)$. Thus, in this case it is appropriate to define some new parameters, which are shown in fig. 6. The new parameters are d, the depth of the bottom of the track (directly below the particle stopping point) and w, the horizontal distance from the bottom of the track to the "back" end of the surface ellipse. The new relations defining these parameters are

$$d = L_r \sin\delta + r - B = L_r (\sin\delta - \sin\theta) \tag{11}$$

and

$$w = L_r \cos\delta + B \tan\tfrac{1}{2}(\delta - \theta). \tag{12}$$

These can be derived by inspection of fig. 6. Of course, the parameters d and w can be used in any case in which the bottom of the vertex sphere is visible from above, not just the nonundercut case. From fig. 3, it can be seen that this is the case if $B > L_r \cos\delta \tan\frac{1}{2}(\delta + \theta)$. It should also be noted that d does not change with etching.

When etching has proceeded to stage (4), as seen in fig. 3, the character of the track is basically the same as after time t_3, except that the vertex sphere portion of the track now just touches the surface of the detector. The value of B necessary to establish this condition is given by

$$B_4 = L_r \left[\sin\theta + \frac{\sin(1/2)(\delta - \theta)}{\cos(1/2)(\delta + \theta)}\right]. \tag{13}$$

As the detector is etched longer than t_4 [stage (4) of fig. 3], the front portion of the surface opening is no longer an ellipse. Rather, it is a portion of a circle formed from the intersection of the vertex sphere with the detector surface.

At this point two new parameters should be defined. The radius of the circular portion of the surface opening is v. From fig. 7 it can be seen that v is given by

$$v^2 = 2 r d - d^2. \tag{14}$$

The total projected length of the opening is no longer 2a. It is now the parameter u, shown in fig. 7. The figure shows that

$$u = L_r \cos\delta + v + B \tan\tfrac{1}{2}(\delta - \theta). \tag{15}$$

As etching proceeds, the circular portion of the surface opening becomes an increasingly greater fraction of the track opening. Before the circular portion becomes a semicircle, however, stage (5) is reached. At etch time t_5 all tracks, even those with $\delta < (\pi/2 - \theta)$, cease to be undercut. As can be seen in fig. 3, this occurs because the etched detector surface has now reached the level of the bottom of the damage trail. Thus B_5 is given by

$$B_5 = L_r \sin\delta. \tag{16}$$

As the etching continues again, the circular portion of the surface opening becomes a semicircle. The point at which this happens can be established by setting b = v. Using eqs. (6), (11), and (14) to eliminate b, r, d, and v, one finds

$$B_6 = L_r (\sin\delta + \sin\theta), \tag{17}$$

where B_6 is the value of B when the surface opening is a semicircle joined to one half of an ellipse. The track is now seen as stage

(6) in fig. 3.

As etching proceeds beyond stage (6), the circular portion becomes greater than a semicircle and the width of the opening is 2v, not 2b.

Finally, with sufficient etching, the track becomes entirely spherical and its surface opening is a circle. This condition is just met when the detector surface has reached the intersection of the etch line for the back of the ellipse and the lower line in fig. 3, which is the locus of the intersection of the conical and spherical track portions. It can be shown that the value of B at this point, B_c, is given by

$$B_c = \frac{L_r \cos\theta}{\tan\frac{1}{2}(\delta - \theta)} . \qquad (18)$$

With $B \geq B_c$, the depth of the track is $d = L_r(\sin\delta - \sin\theta)$ and the radius of its circular opening is $v = \sqrt{d(2B - B_6)}$.

4. Track Specification and Measurement Parameters

The situations shown in figs. 4 through 7 can be completely specified by not more than four parameters. The four parameters that are most useful are δ, θ, L_r, and B. Of course, for pointed tracks L_r is replaced by L. All other quantities of interest can be computed quite easily and directly from these four parameters.

Since some (or in some cases all) of the above specification parameters cannot be measured directly, they must be computed from parameters that can be measured. The parameters that can be measured easily for a single track are: for undercut tracks, s, a, b, z, and r; and for nonundercut tracks, w, d, v, and u.

In some cases one or two of the specification parameters can be

measured. If the damage trails were produced by exposing the detector to a collimated particle beam of known dip angle or if the two tracks produced by the same particle on the opposite surfaces of the detector can be measured, δ is known quite accurately. It is also possible to measure B (for damage trails intersecting the surface of the detector prior to etching) by measuring the sample thickness or weight before and after etching and applying appropriate corrections for the edge effects.

With the two specification parameters described in the last paragraph there are seven possible measurement parameters--δ, B, s, a, b, z, and r--that can be used to derive the four specification parameters δ, θ, L_r, and B for undercut tracks. Since only four measurements are necessary to determine the specification parameters, the set of measurement variables yielding the greatest accuracy or possibly the greatest measurement facility should be chosen for each particular situation. This paper strives to make this possible by giving the specification parameters in terms of seven different sets of measurement parameters. These seven sets are given in table 1. The sets are also applicable to pointed tracks if r is set equal to zero and L_r is replaced by L. Of course if more than four parameters are measured, a least-squares fitting procedure can be used to obtain the best values of the specification parameters. However, this is beyond the scope of the present paper.

The specification parameters can also be computed from the measurement of tracks that are not undercut (sets 8 and 9). Set 8 uses the measurement parameters a, b, w, and d and is applicable for $L_r \cos\delta \tan\frac{1}{2}(\delta + \theta) < B < B_4$. Set 9 uses the measurement parameters u, v, b, and d and is applicable for $B_4 < B < B_6$.

4.1. Measurement optimization

The accuracy of the computed specification parameters can be maximized by choosing the appropriate set of measurment parameters. The following discussion indicates the situation in which each of the measurement sets is most useful.

If δ is known accurately, one of the sets 1 through 4 should be used. Sets 1 and 2 are easy to use since it is only necessary to measure B once for a surface. Sets 3 and 4 are more accurate for tracks with small θ values because they allow for a variation of B over the detector surface, but when θ is large, b is small and thus subject to a greater measurement error. For large θ tracks, sets 1 and 2 are better suited. Also it is possible to apply sets 1 and 2 only to tracks produced by damage trails intersecting the surface prior to etching. For the greatest accuracy, sets 1 and 3 should be used for shallow tracks (small δ values) and sets 2 and 4 for steep tracks (large values of δ). In fact, since s is considerably easier to measure than z, sets 2 and 4 should be used only where tracks are quite steep.

When the value of δ is not known, sets 5, 6, and 7 must be used. Set 5 is more accurate, particularly for steep tracks. Set 6 is easier to measure because $\underline{a}$ is more easily measured than z, but it should not be applied to steep tracks. It should be noted that all the variables measured in set 6 are in the horizontal plane. Thus it is possible to measure a track from a photomicrograph. Set 7 has the advantages of not requiring the measurement of b for every track and of greater accuracy if θ is large.

For tracks that are not undercut, only one set of measurement parameters is available for each case. It should also be noted that

although in principle set 8 can always be used to obtain the specification parameters, in practice it is useful only for tracks with relatively large values of θ and values of δ somewhat different than $\pi/2$, so that $a \neq b$. However, if it can be seen that $r = 0$ (only a small point of light in the center of the dark track as observed with an optical microscope), w and d become s and z, and set 5 can be used with good accuracy for all values of δ and θ.

5. Sets of equations relating specification to measurement parameters

Equations (5), (6), (8), (9), (10), (11), (12), (14), and (15) can be used to derive the nine sets of relations for the specification parameters. In all cases except two these relations are explicit. The two implicit relations for θ can be solved by iteration. In most cases, four or five iterations suffice for the convergence of θ if the initial value is $\theta = 0$. In extreme cases (large θ), these relations must be solved by interpolation or by Newton's method, in which case the convergence is more rapid.

Set 1: δ, B, s, and r

For this set δ and B are measured directly,

$$\sin\theta = \frac{(B - r)\cos\delta}{s - r - B\tan\frac{1}{2}(\delta - \theta)} \tag{19}$$

is iterated for θ,

and $$L_r = \frac{s - r - B\tan\frac{1}{2}(\delta - \theta)}{\cos\delta} . \tag{20}$$

Set 2: δ, B, z, and r

For this set δ and B are measured directly,

$$L_r = \frac{z + B}{\sin\delta} , \tag{21}$$

and $$\sin\theta = \frac{B - r}{L_r} . \qquad (22)$$

Set 3: δ, s, b, and r

For this set δ is given,

$$\sin\theta = \frac{b\cos\delta\sin\delta - r\cos\delta\sqrt{\sin^2\delta - \sin^2\theta}}{(s-r)\sqrt{\sin^2\delta - \sin^2\theta} - b\cos\theta} \qquad (23)$$

is iterated for θ, and B is obtained from eq. (6) and L_r from eq. (20). It should be noted that in set 3 there are two possible solutions. Most probably in real cases the one with the smaller value of θ is correct. The computed value of B can be used as a test.

Set 4: δ, b, z, and r

For this set δ is given,

$$\sin\theta = \left(\frac{b\sqrt{z^2 + b^2 - r^2} - z\,r}{z^2 + b^2}\right)\sin\delta, \qquad (24)$$

$$L_r = \frac{z + r}{\sin\delta - \sin\theta} , \qquad (25)$$

and B is obtained from eq. (8).

Set 5: s, b, z, and r

First $(\delta-\theta)$ and $\sin\theta/\sin\delta$ are given by

$$\sin(\delta-\theta) = \frac{r(s-r) + z\sqrt{s^2 - 2sr + z^2}}{(s-r)^2 + z^2} \qquad (26)$$

and

$$\frac{\sin\theta}{\sin\delta} = c = \frac{b\sqrt{z^2 + b^2 - r^2} - z\,r}{z^2 + b^2} . \qquad (27)$$

Then the specification parameters are computed by

$$\tan\theta = \frac{c\sin(\delta-\theta)}{1 - c\cos(\delta-\theta)} , \qquad (28)$$

$$\delta = (\delta-\theta) + \theta. \qquad (29)$$

Set 6: δ, a, b, and r

For this set

$$\tan\theta = \left(\frac{\sqrt{a^2 - b^2}}{a}\right)\frac{\sqrt{b^2(s-r-a)^2 - (a^2-b^2)(b^2-r^2)} - r(s-r-a)}{(s-r-a)^2 - (a^2 - b^2)} , \qquad (30)$$

$$\sin\delta = \frac{\sqrt{a^2\sin^2\theta + b^2\cos^2\theta}}{a} , \qquad (31)$$

$$L_r = \frac{s-r-a + \sqrt{a^2 - b^2}}{\cos\delta} . \qquad (32)$$

and B is obtained from eq. (8).

Set 7: B, s, z, and r

For this set B is known, $\sin(\delta-\theta)$ is obtained from eq. (26),

$$\frac{\sin\theta}{\sin\delta} = c = \frac{B - r}{B + z} , \qquad (33)$$

and $\tan\theta$, δ, and L_r are respectively obtained from eqs. (28), (29), and (21).

Set 8: a, b, w, and d

For this set

$$\tan\theta = \frac{b^2\left[w - a + \sqrt{a^2-b^2}\right]^2 - d^2(a^2-b^2)}{2\,a\,d\sqrt{a^2-b^2}\,(w-a+\sqrt{a^2 - b^2})} , \qquad (34)$$

$\sin\delta$ is obtained from eq. (31),

$$L_r = \frac{d}{\sin\delta - \sin\theta}, \tag{35}$$

and $$B = \frac{a(\sin\delta + \sin\theta)}{\cos\theta}. \tag{36}$$

Set 9: u, v, b, and d

If auxiliary variables are given by

$$r = \frac{v^2 + d^2}{2d}, \tag{37}$$

$$h = \frac{d}{u - v}, \tag{38}$$

$$\lambda = \frac{r(r-d) + b\sqrt{b^2 - 2rd + d^2}}{b^2 + (r-d)^2}, \tag{39}$$

and

$$\xi = \frac{\lambda d + (1-\lambda) r}{u - v}, \tag{40}$$

the specification parameters are given by

$$\tan\delta = \frac{(1+\lambda)h + \xi\sqrt{1 + \frac{(1+\lambda)h^2}{(1-\lambda)} - \frac{2\xi h}{(1-\lambda)} - \xi}}{(1 - \lambda^2 - \xi^2)}, \tag{41}$$

$$\sin\theta = \lambda \sin\delta, \tag{42}$$

L_r is obtained from eq. (35) and B from eq. (8).

6. Computation of the Track Etch Rate

The most useful and important parameter that can be computed from the specification parameters is the track etch rate, V_T. In terms of the bulk etch rate V_G, it is given by eq. (1). If a damage trail, known to have intersected the surface prior to etching, is etched to form a track and the total etch time is t, V_T is given more accurately if V_G in eq. (1) is given by

$$V_G = \frac{B}{t}, \tag{43}$$

where B has the value consistent with the parameters of the particular track being measured.

6.1. Track measurement

It has been assumed throughout this paper that all the parameters used were the real physical parameters in a consistent set of units. Scale factors and the corrections for index of refraction in the z measurement are peculiar to the particular measurement situation and will not be discussed here. However, there are several pertinent points to be noted.

All the measurement parameters are defined in such a way that no "guesswork" is necessary to measure them. For example, it is not necessary to estimate the point of intersection of the particle trajectory and the surface (it is not the center of the surface ellipse but lies a distance $\frac{a\tan\theta}{\tan\delta}$ toward the "front" end of the ellipse).

The parameters s, a, u, and b are all measured between two track "boundaries." To obtain z, the microscope is alternately focused on the detector surface and the very end of the vertex or tip, even if rounded. If θ is small, r can be taken to be half the diameter of the vertex. If θ is large (but $> \frac{\pi}{4}$), it can be measured by making two perpendicular reticule lines tangent to the vertex sphere (as projected onto the horizontal plane) and finding the distance from the point of tangency to the intersection of the reticule lines. This distance is r.

The parameters v and w are measured from a track boundary to the center of the small circle of light seen at the bottom of the track. This circle of light is the virtual image of the microscope condenser diaphragm formed by the track vertex sphere.

We acknowledge the valuable assistance given by Dr. C. A. Tobias and Dr. T. A. Parnell.

References

1) Proceedings of the International Topical Conference on Nuclear Track Registration in Insulating Solids and Applications (Clermont-Ferrand University Press, 1969).

2) Proceedings of the Seventh International Colloqium on Corpuscular Photography and Visual Solid Detectors, Barcelona, 1970 (in press).

3) E. V. Benton, A study of charged particle tracks in cellulose nitrate, USNRDL-TR-68-14, 1968.

TABLE 1

Sets of measurement variables for undercut tracks

Set No.	Measurement variables						
1	δ	B	s	-	-	-	r
2	δ	B	-	-	-	z	r
3	δ	-	s	-	b	-	r
4	δ	-	-	-	b	z	r
5	-	-	s	-	b	z	r
6	-	-	s	a	b	-	r
7	-	B	s	-	-	z	r

Figure Captions

Fig. 1. Damage trail and track etching on a sub-microscopic scale.

Fig. 2. Partially etched particle damage trails seen on the scale of an optical microscope. Both tracks are etching toward the right-hand side of the figure. It should be noted that the diameter of the damage trail has been exaggerated.

Fig. 3. Sequential stages of track etching for a particle damage trail of finite length.

Fig. 4. Pointed tracks and their parameters ($B < L_r \sin\theta$).

Fig. 5. Rounded tracks and their parameters

$$\left(L_r \sin\theta < B < L_r\left[\sin\theta + \frac{\sin(1/2)(\delta - \theta)}{\cos(1/2)(\delta+\theta)}\right]\right).$$

Fig. 6. Tracks with no undercutting and their parameters ($\delta > \frac{\pi}{2} - \theta$).

Fig. 7. Nonundercutting tracks with partially circular track openings and their parameters.

($L_r \sin\delta < B < L_r[\sin\delta + \sin\theta]$).

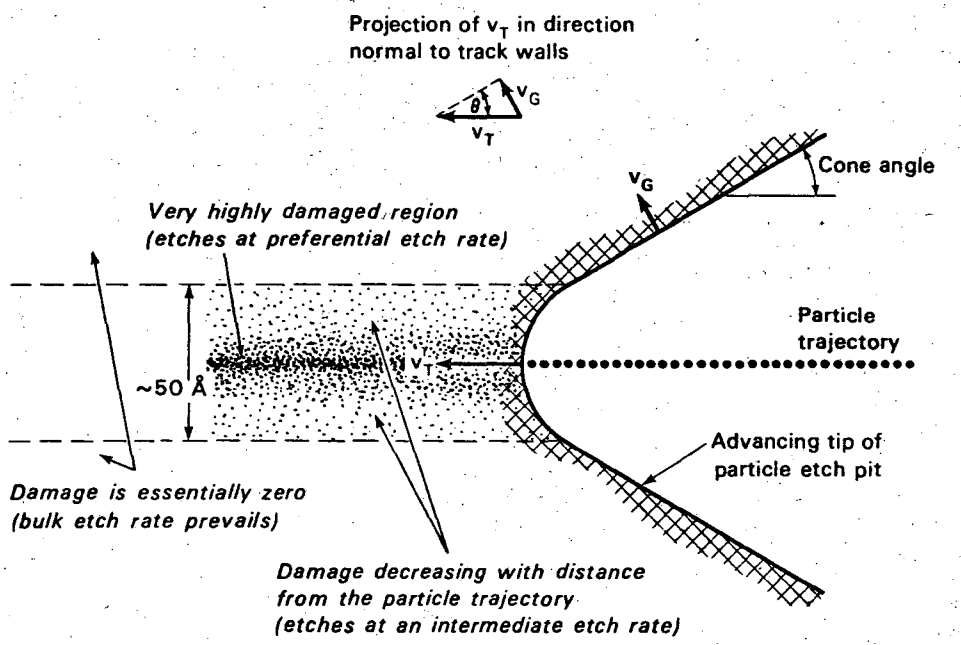

Fig. 1

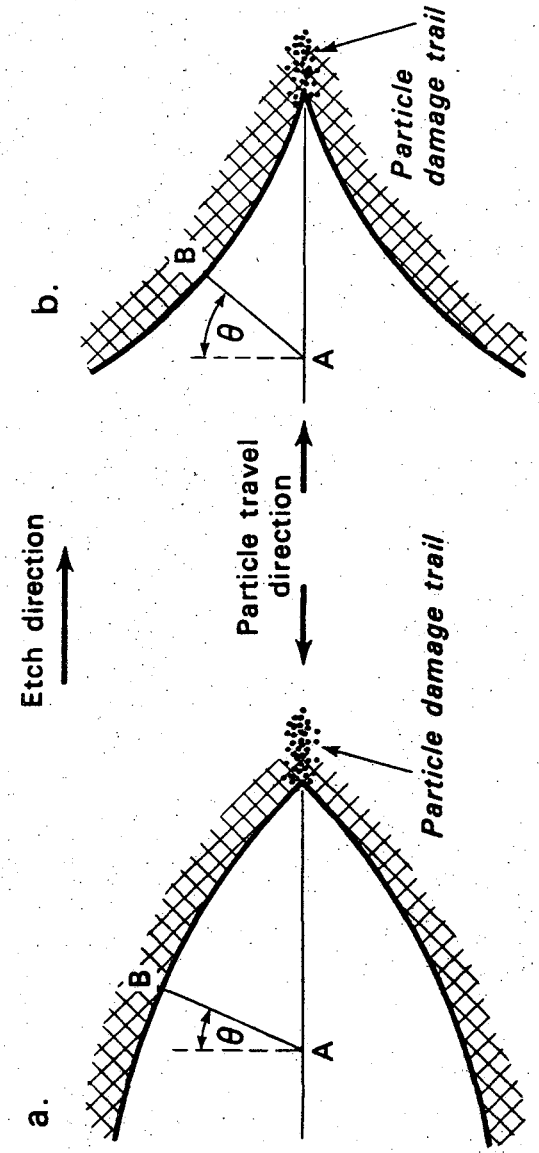
b.
Particle damage trail
B
θ
A
Etch direction
Particle travel direction
Particle damage trail
a.
Particle damage trail
B
θ
A

Fig. 2

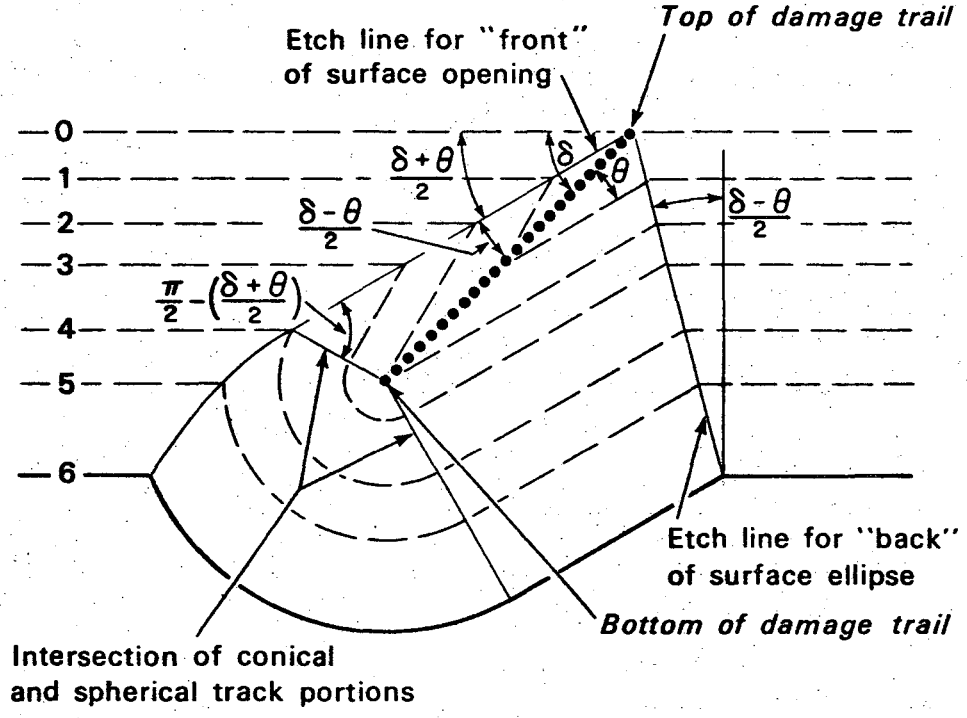
Top of damage trail
Etch line for "front" of surface opening
0
1
2
3
4
5
6
$\frac{\delta+\theta}{2}$
$\frac{\delta-\theta}{2}$
$\frac{\pi}{2}-\left(\frac{\delta+\theta}{2}\right)$
δ
θ
$\frac{\delta-\theta}{2}$
Etch line for "back" of surface ellipse
Bottom of damage trail
Intersection of conical and spherical track portions

Fig. 3

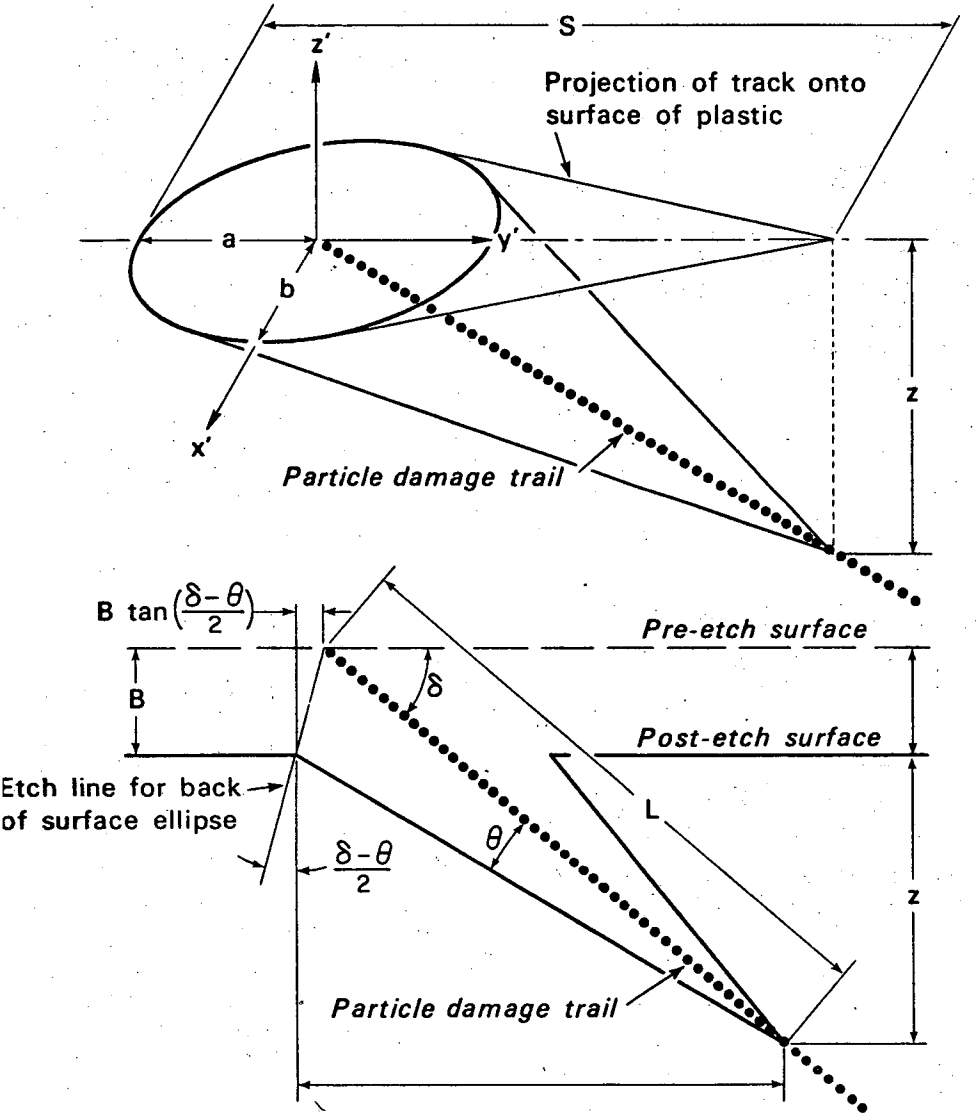
S
z'
Projection of track onto
surface of plastic
a
y'
b
x'
z
Particle damage trail
B tan(δ-θ/2)
Pre-etch surface
B
δ
Post-etch surface
Etch line for back
of surface ellipse
L
θ
δ-θ/2
z
Particle damage trail

Fig. 4

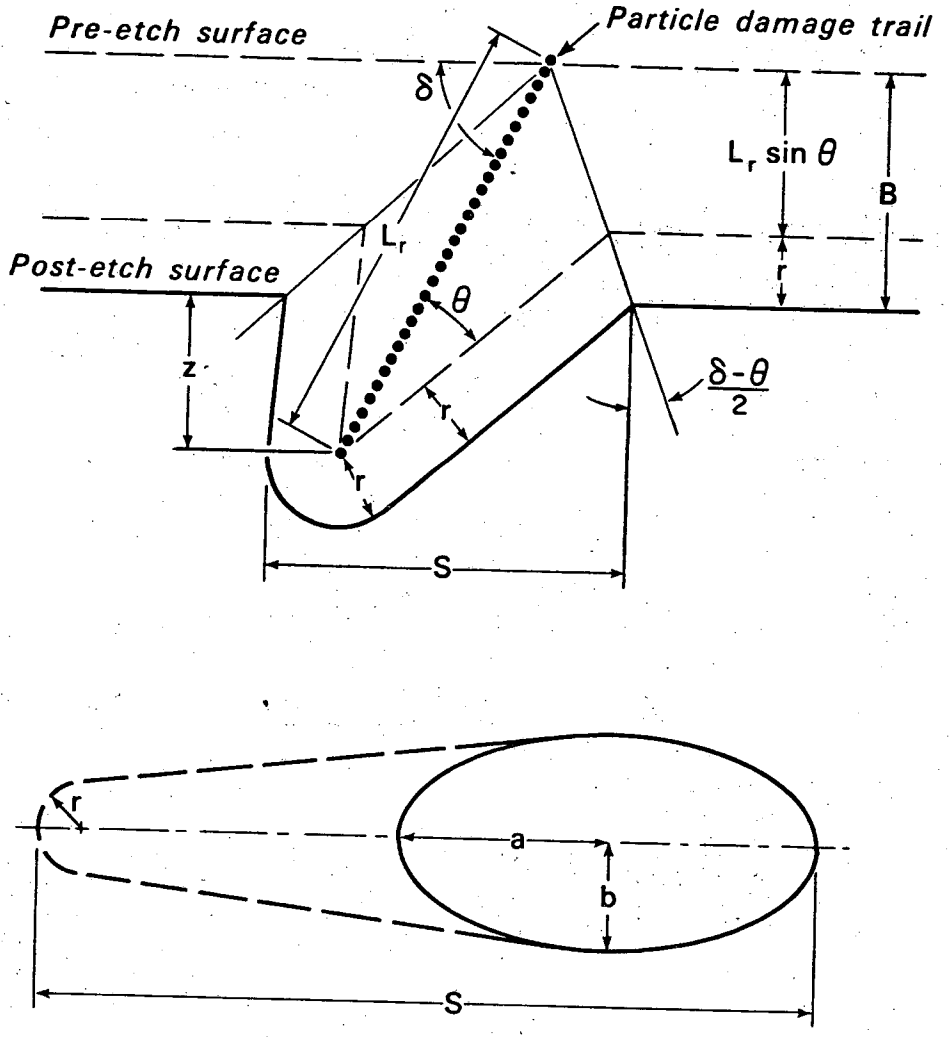
Pre-etch surface
Particle damage trail
δ
L_r sin θ
B
L_r
Post-etch surface
θ
r
z
δ-θ/2
r
r
S
r
a
b
S

Fig. 5

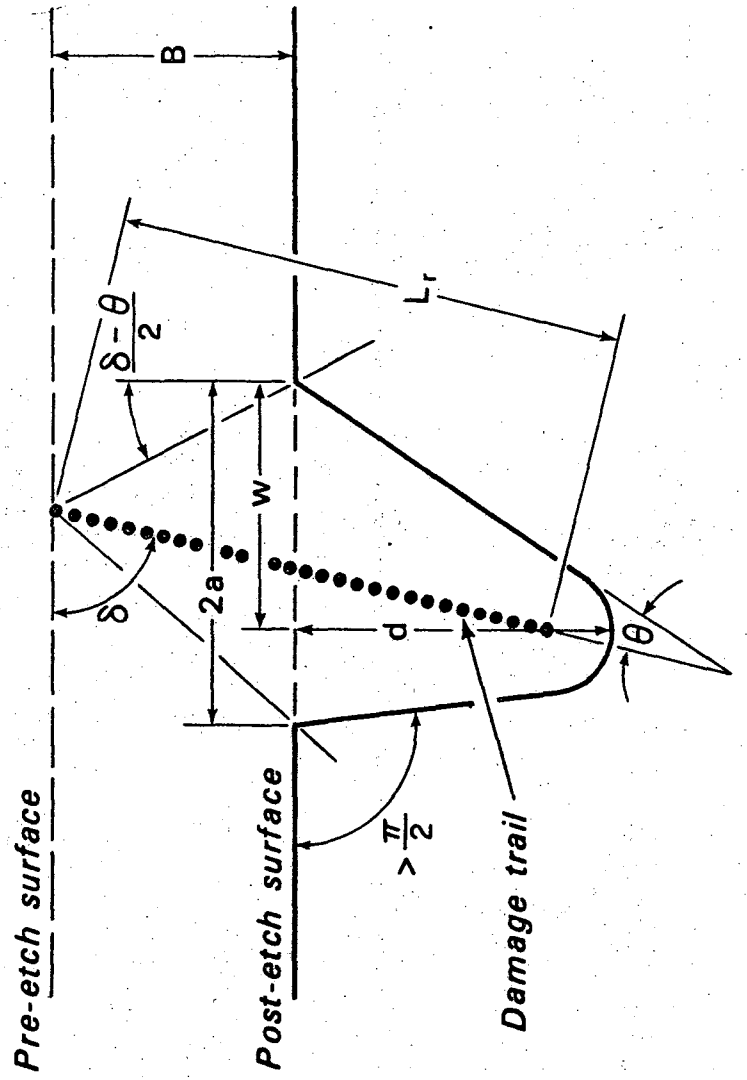
B
L_r
$\frac{\delta-\theta}{2}$
w
2a
d
δ
θ
$\frac{\pi}{2}$
Pre-etch surface
Post-etch surface
Damage trail

Fig. 6

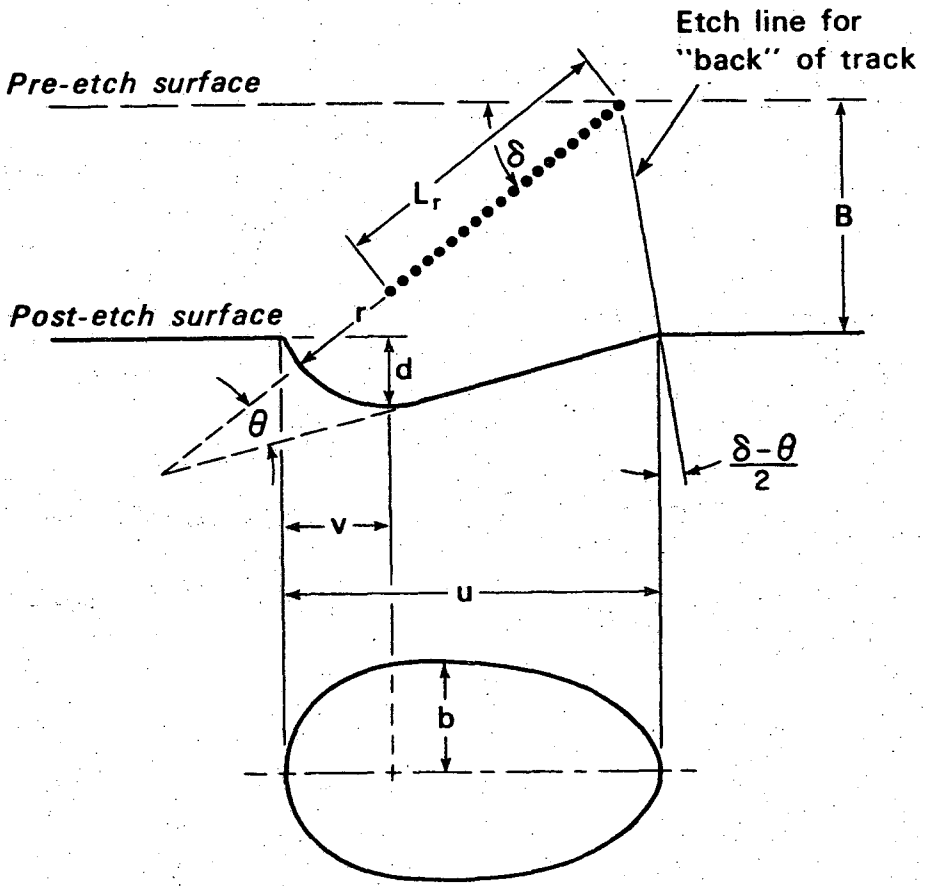
Etch line for "back" of track
Pre-etch surface
Post-etch surface
L_r
δ
r
B
d
θ
$\frac{\delta-\theta}{2}$
v
u
b

Fig. 7

TECHNICAL INFORMATION DIVISION
LAWRENCE BERKELEY LABORATORY
UNIVERSITY OF CALIFORNIA
BERKELEY, CALIFORNIA 94720